Energy Migration Dynamics in a Ru(II)- and Os(II)-Based Antenna Polymer Embedded in a Disordered, Rigid Medium

Cavan N. Fleming, Paul Jang, Thomas J. Meyer,* and John M. Papanikolas*,†

Department of Chemistry, Venable and Kenan Laboratories, University of North Carolina at Chapel Hill, Chapel Hill, North Carolina 27599-3290

Received: August 25, 2003

The energy migration dynamics have been studied in multi-centered assemblies embedded in poly(methyl methacrylate) (PMMA) films using steady-state and time-resolved emission techniques. The assemblies consist of twenty Ru(II) and Os(II) polypyridyl coordination complexes linked through a polystyrene backbone. Energy migration is initiated by photoexcitation of one of the Ru(II) sites and terminated upon sensitization of a low-energy Os trap. The inhomogeneous environment of the assembly results in a distribution of excited-state energies, which is frozen in time due to the rigidity of the PMMA film. Energy migration proceeds toward the lower energy sites, resulting in a time-dependent red-shift in the polymer emission band.

I. Introduction

The ability of polymers to conduct excited-state energy is well documented.[1−11] There are many examples of multi-centered systems in which photoexcitation initially produces a localized excited state that then migrates between pendent chromophores by Dexter or Forster energy transfer. In fluid solution, the presence of fast solvent relaxation and a homogeneous environment leads to energy migration between chromophores that are thermally equilibrated and, if chemically identical, isoenergetic.

We have recently published results on the excited-state energy migration dynamics within a supramolecular assembly containing polypyridyl Ru(II) and Os(II) chromophores.[11] The chromophores are linked through a polystyrene backbone to yield assemblies with approximately 20 coordination complexes (17 Ru^{II} and 3 Os^{II}) per chain. The chemical structures of the polymer and monomer constituents are shown in Figure 1. Energy migration is initiated upon photoexcitation of the metal-to-ligand charge-transfer transition (MLCT) of one of the Ru sites, which then leads to efficient energy transport to a lower energy Os trap through a series of Ru* → Ru energy hops. The macromolecular structure of the assembly plays an important role in its energy transport properties. Figure 1 depicts a structure calculated using Monte Carlo simulation methods. Here, the larger spheres are the Ru^{II} or Os^{II} chromophores and the smaller spheres are the PF_6^- counterions that surround the polymer whose overall charge is +40. The polymer adopts a twisted backbone and extended rodlike structure that attempts to alleviate the steric and Coulombic repulsions between adjacent chromophores, and the result is a densely packed structure in which the average distance between the peripheries of adjacent chromophores is 2−3 Å. Our previous work[11] shows efficient energy transport along the polymer chain, which is facilitated by the close proximity of the pendent groups.

We report here results on the incorporation of these supramolecular assemblies into room-temperature solid solutions. Like its fluid solution counterpart, steady-state and time-resolved emission studies indicate that this antenna polymer is capable of energy transport, even when it is embedded in poly(methyl methacrylate) (PMMA) films. This paper explores the effect of the rigid environment on the energy transport process.

One benchmark for comparison is electron transfer reactions, which are sensitive to the dynamical response of the surrounding medium. Solvent molecules reorient in response to the changing charge distribution between the donor and acceptor. In rigid media, where solvent motion is restricted, the energetics and dynamics of electron transfer reactions are significantly effected, often to the point where the reaction is shut down.[12,13] Unlike electron transfer, the nature of the solvent should play a less prominent role for energy transfer, since energy transfer involves the motion of a dipole, as opposed to individual charges. This role is not necessarily negligible, however, given the sensitivity of the energetics of charge-transfer excited states toward the solvent environment.

Our results point to additional complexities arising from this solid surroundings. These complexities are manifested as (1) nonexponential decay kinetics in the monomers and homopolymers ($PS-Ru_{20}$ and $PS-Os_{20}$), (2) spectroscopic differences between the monomers and their corresponding homopolymers, and (3) time-dependent spectral shifts in the emission spectra of the polymers. All of these are qualitatively different from our observations in fluid solutions, and stem from a combination of two factors: a lifting of degeneracy of adjacent excited states due to inhomogeneities in the local electrostatic field and the rigid molecular environment. As a result, excited states migrate toward lower energy sites and can become trapped at electrostatic minima. Although inhomogeneities are also present in fluid solution, the motion of adjacent sites relative to each other causes the energy of a particular site to fluctuate, and this prevents trapping. Our conclusions have implications for describing energy transport in fluid solutions. In particular, it suggests that the efficient energy migration observed in fluid solution might arise (at least in part) from a trapeze-like motion of the side chains that brings adjacent sites into close physical contact, thus enhancing the overlap of donor and acceptor wave functions. If this is the case, then inter-site motion and flexibility

* Authors to whom correspondence should be addressed.
† E-mail: John_Papanikolas@unc.edu.

10.1021/jp0365312 CCC: $27.50
Published on Web 01/22/2004

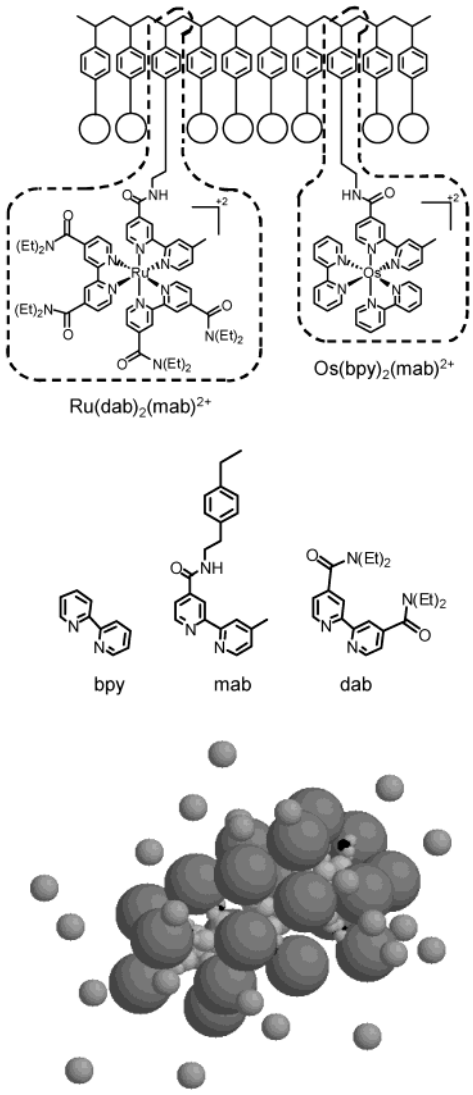

Figure 1. Chemical structures of the monomer and polymer systems discussed in this work (top) and a three-dimensional view of the polymer system obtained from Monte Carlo simulation (bottom), ref 11.

would be an important architectural feature that is needed to design efficient nanoscale materials for energy transport.

II. Experimental Section

Preparation of Polymer Films. An amount of 0.6 g of PMMA was dissolved in 5 mL of chloroform. Dissolution occurred over a period of ~30 min with constant stirring and mild heat (~40 °C) applied. The PF_6^- salt of the complex or polymer array was dissolved in chloroform or acetonitrile, depending upon its solubility, and its concentration was adjusted to achieve an OD of ~0.6 at the MLCT maximum. An amount of 1 mL of the complex solution was added to the polymer solution, stirred, and poured into a Teflon mold. The solvent was allowed to evaporate slowly over a period of 2−3 days in an open-air desiccator. The resulting film was then placed in a vacuum desiccator for 2 days prior to making measurements. The films produced were 4 cm in length and 1 cm in width, and had a fairly uniform thickness of ~1 mm.

Measurements. UV−visible spectra were recorded on a diode array spectrometer with 2 nm resolution. The spectroscopic grade acetonitrile used in the photophysical measurements was either used as received or distilled over CaH_2. Steady-state emission spectra were recorded on a photon counting spectrofluorimeter and were corrected for the instrument response. Optically dilute samples (less than 0.12 OD at the excitation wavelength) were argon sparged for 40 min prior to use. Measurements in rigid media were performed in open atmosphere. Emission quantum yields were calculated by relative actinometry using eq 1.

$$\Phi_{sam} = \Phi_{ref}\left(\frac{I_{sam}}{I_{ref}}\right)\left(\frac{n_{sam}}{n_{ref}}\right)^2\left(\frac{A_{ref}}{A_{sam}}\right) \quad (1)$$

In this equation, Φ_{sam} is the emission quantum yield of either the sample or the reference compound, I is the integrated emission profile, n is the refractive index of the solvent, and A is the absorbance of the sample in a 1 cm quartz cuvette or in ~1 mm PMMA films drip-coated onto a quartz plate. For fluid solution measurements, the reference was either $[Ru(bpy)_3](PF_6)_2$ for which $\Phi_{ref} = 0.062$ or $[Os(bpy)_3](PF_6)_2$ for which $\Phi_{ref} = 0.005$ in acetonitrile at 298 K. The reference used for measurements in PMMA is [Rhodamine 6G](Cl) in PMMA at 298 K for which $\Phi_{ref} = 0.77$. The reference quantum yield used here is the average of two published values.[14,15]

Time-resolved measurements were conducted by time-correlated single-photon counting (TCSPC). The apparatus consists of a commercially available mode-locked Nd:YAG laser whose frequency-tripled output is used to synchronously pump a single jet dye laser with Stilbene 3. The dye laser output at 430 nm is cavity dumped to produce ~10 ps pulses with ~6 nJ/pulse energies. The repetition rate of the dye laser was selected to be roughly 5 times the natural lifetime of the sample (475 kHz for measurements at 780 nm or 190 kHz for measurements at 640 nm at room temperature). The beam is passed through an iris and illuminated without focusing a 10 mm quartz cuvette. The intensity of the detected luminescence is varied by use of ND filters mounted before the monochromator. For luminescence measurements the emitted light is collected at 90° and focused onto the slit of a 240 mm focal length, single grating monochromator and subsequently delivered to a cooled, multichannel plate-photomultiplier tube (MCP-PMT) with a 170 ps rise time. The signal from the MCP is amplified prior to sending it into a 200 MHz constant fraction discriminator (CFD) whose output served as the start pulse for the time-to-amplitude converter (TAC). The stop pulse in the timing scheme is obtained by splitting off 10% of the excitation beam and focusing it onto a photodiode. The photodiode pulse is sent into a variable delay box, then to the CFD, and finally to the TAC. The TAC's output is processed by a multichannel analyzer that is interfaced to a PC. The time-resolution of the apparatus is ~100 ps.

III. Results and Discussion

In a previous report on the energy transfer dynamics in room-temperature CH_3CN,[11] we combined steady-state and time-resolved spectroscopy with Monte Carlo simulations to obtain a detailed look at the polymer structure and its relationship to the energy transfer dynamics in $PS-Ru_{17}Os_3$. In this paper we extend the fluid solution work to an amorphous solid, PMMA.

As with the fluid solution, the energy transport properties will be closely linked to the macromolecular structure of the polymer array. Given the dense loading of complexes, we expect that the polymer array will adopt a similar extended rodlike structure in PMMA as it does in CH_3CN. However, some differences may exist. In the low dielectric environment of PMMA ($D_s = 3.6$) the counterions are more closely associated with the assembly. Furthermore, in the absence of a small, highly

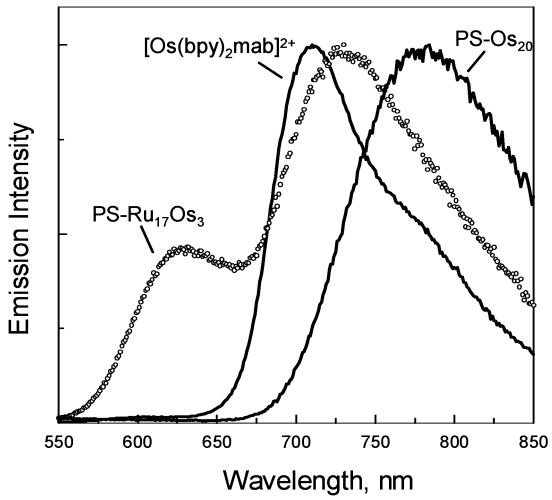

Figure 2. Steady-state emission spectra of $[Os(bpy)_2(mab)]^{2+}$, PS−$Ru_{17}Os_3$, and PS−Os_{20} in room-temperature PMMA. Excitation was at 423 nm.

polar solvent such as CH_3CN, the electrostatic interactions between adjacent complexes could be greater, and this would increase the average periphery−periphery distance. Beyond these small differences, the polymer arrays can be accurately described as a densely loaded system in which each site is in close proximity to multiple neighbor sites.

The discussion of our spectroscopic results is divided into two sections. Section A describes our steady-state results, while time-resolved results are presented in Section B.

A. Steady-State Emission. Steady-state emission spectra of $[Os(bpy)_2(mab)]^{2+}$, PS−Os_{20}, and PS−$Ru_{17}Os_3$ embedded in room-temperature PMMA are displayed in Figure 2. These spectra differ from their fluid solution counterparts in several regards.

The changes observed for the monomer complexes are consistent with trends expected for rigid media. The emission band of $[Os(bpy)_2(mab)]^{2+}$, which peaks at 715 nm, is shifted to higher energy in rigid polymeric media relative to its value in CH_3CN where $\lambda_{max} = 780$ nm. Furthermore, the band is not as broad and has more structure than it does in fluid solution; vibronic structure appears at ∼775 nm in PMMA. These observations are typical for emissive MLCT excited states in rigid environments.[16,17] The origin of this blue shift is also well understood. In fluid solution, the solvent dipoles reorient to configurations appropriate to the electronic configuration of the excited state, stabilizing the excited state, and leading to a red-shifted emission band. In rigid solvents, the medium is at least partially frozen on the time scale for excited-state decay; emission then occurs with the surrounding solvent dipole orientations more like those surrounding the ground state and the emission appears at higher energy. Emission quantum yields are also consistent with this picture (Table 1). The quantum yields of both Ru and Os complexes *increase* upon incorporation into PMMA, consistent with the higher excited-state energy, as predicted by the energy gap law.

While the monomer emission is consistent with other observations in rigid environments, the polymer emission is not. In fluid solution, the homopolymers (PS−Ru_{20} and PS−Os_{20}) are spectroscopically equivalent to their corresponding monomer complexes. However, in PMMA there are stark differences between the two. PS−Os_{20} in PMMA has an emission band typical of fluid acetonitrile, and the Os* emission from PS−$Ru_{17}Os_3$ is intermediate between these two cases (Figure 2). In addition, the increase in quantum yield observed upon incorporation of the monomer into the rigid environment is not observed for the polymers. On the whole, comparison between the PMMA and CH_3CN results suggest that while the spectroscopic properties of the monomer change upon incorporation into the PMMA matrix, consistent with known rigid media effects, the polymer arrays have spectroscopic properties that remain more akin to those observed in fluid solution. These observations can be explained by a dispersion in the Os* excited-state energies, which is discussed in more detail in Section B.

TABLE 1: Summary of Room Temperature Lifetimes (τ) and Emission Quantum Yields (Φ_{em}) in PMMA and CH_3CN

	CH_3CN[c]		PMMA[c]	
complex	Φ_{em}	τ (ns)	Φ_{em}	τ (ns)
$[Ru(dab)2(mab)]^{2+}$	0.11	1100[a]	0.21	1490[a]
PS−Ru20	0.10	1000[a]	0.050	1200[b]
$[Os(bpy)2(mab)]^{2+}$	0.0030	56[a]	0.030	140[a]
PS−Os20	0.0032	49[a]	0.0027	40[b]

[a] A sum of two exponential functions was used to fit the decays. The results are as follows: $\tau_1 = 87$ ns (0.42), $\tau_2 = 182$ ns (0.55) for $[Os(bpy)_2(mab)]^{2+}$; $\tau_1 = 650$ ns (0.30), $\tau_2 = 1850$ ns (0.70) for $[Ru(dab)_2(mab)]^{2+}$. Average lifetimes are reported. Monitoring occurred at the emission band maximum. [b] A sum of three exponential functions was used to fit the decays. The results are as follows: $\tau_1 = 2$ ns (0.20), $\tau_2 = 13$ ns (0.40), $\tau_3 = 40$ ns (0.35) for PS−Os_{20}; $\tau_1 = 20$ ns (0.15), $\tau_2 = 225$ ns (0.20), $\tau_3 = 1200$ ns (0.60) for PS−Ru_{20}. Slow component is tabulated for two polymers samples. Spectral evolution is observed on the 1−10 ns time scale which is partly responsible for the nonexponential behavior observed in the PS−Os_{20} and PS−Ru_{20}. This evolution does not reflect the emissive properties of the complexes, but rather energy migration among complexes with an inhomogeneous distribution of excited-state energies. Monitoring occurred at the emission band maximum. [c] Care must be taken in making quantitative comparisons between the two different solvents (PMMA versus CH_3CN) because different references were used, and each reference is most likely known to differing degrees of certainty.

B. Time-Resolved Emission. This project examines the time-resolved emission from the mixed loaded polymer, PS−$Ru_{17}Os_3$, the homopolymers, PS−Ru_{20} and PS−Os_{20}, and the corresponding monomers, $[Os(bpy)_2(mab)]^{2+}$ and $[Ru(dab)_2(mab)]^{2+}$ in room-temperature PMMA. The monomers and homopolymers serve as model systems for the mixed loaded system.

Energy transport along the polymer backbone is evident in the time-resolved emission data obtained from the PS−$Ru_{17}Os_3$/PMMA samples. Figure 3 shows the growth and decay of Os emission (observed at 780 nm) and the decay of the Ru emission (observed at 640 nm) as a function of time after photoexcitation of the Ru sites in PS−$Ru_{17}Os_3$. The delayed growth in the Os emission, and its correlation with the Ru decay, is a clear indication of Os sensitization by Ru excited states. The time scale associated with the growth of the Os emission reflects both the rates of individual Ru* → Ru energy transfer events and the number of steps needed to reach the Os trap. Qualitatively the Os* rise kinetics are similar in PMMA and acetonitrile. In acetonitrile a fast, instrument response limited rise comprises ∼55% of the signal. The fast rise has contributions from both direct Os excitation and Ru emission (detected as a result of the overlapping emission bands at 780 nm) as previously discussed.[11] In PMMA the fast rise appears to be a larger fraction of the signal, 60−70%. This could be indicative of a lower efficiency for energy transport compared with fluid solution; however, a quantitative measure based on the time-resolved data was not possible.

In our fluid solution studies, we were able to determine the contribution of direct Os excitation and Ru emission to the fast

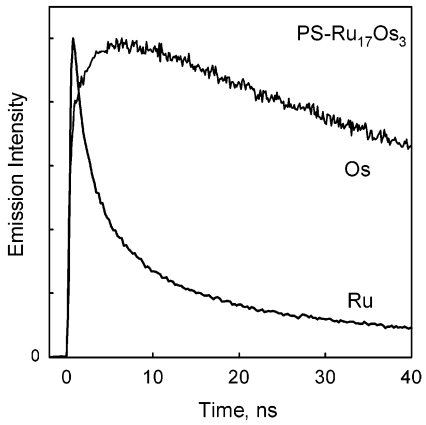

Figure 3. Time-resolved emission detected from PS−$Ru_{17}Os_3$ in room temperature PMMA while monitoring at 730 nm. The transient shown is an average of three measurements made from three different samples. In all cases we observe sensitized Os emission, but the exact kinetics of the rise vary slightly between samples, unlike our observations in fluid solution.

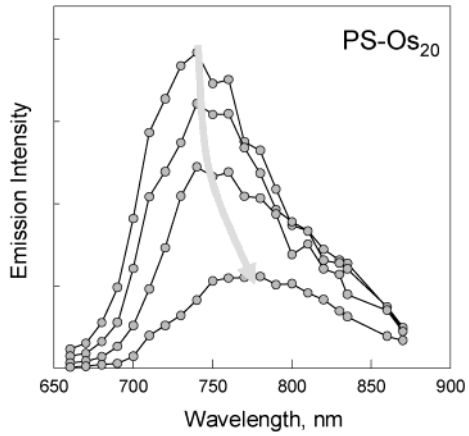

Figure 4. Time-resolved emission spectra of PS−Os_{20} in room-temperature PMMA. Spectra have been corrected for the instrument response. Spectra measured at t = 110 ps, 510 ps, 2 ns, and 10 ns (from top to bottom).

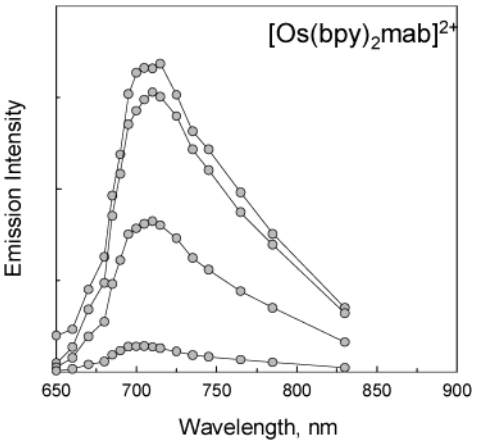

Figure 5. Time-resolved emission spectra of $[Os(bpy)_2(mab)]^{2+}$ in room-temperature PMMA. Spectra have been corrected for the instrument response. Spectra measured at t = 0, 10, 100, and 400 ns (from top to bottom).

rise and use this information to assess the energy transfer efficiency in CH_3CN. This was possible in part because in fluid solution the monomer complexes, $[Ru(dab)_2(mab)]^{2+}$ and $[Os(bpy)_2(mab)]^{2+}$, are spectroscopically equivalent to their corresponding homopolymers, PS−Ru_{20} and PS−Os_{20}. This is not the case in the rigid polymeric media where the excited-state energies, lifetimes, and emission quantum yields for Os emission in PS−Os_{20}, the mixed polymer PS−$Ru_{17}Os_3$, and $[Os(bpy)_2(mab)]^{2+}$ are all different (Table 1).

While there are qualitative similarities in the kinetics found in fluid solution versus PMMA, there are some significant differences. In fluid solution, both the monomers and homopolymers show nearly identical spectroscopic signatures. Both exhibit single-exponential decay kinetics with similar decay rates, and the emission spectra decay without a change in shape (i.e., kinetics are independent of monitoring wavelength). In PMMA, on the other hand, the correspondence between the monomer and its corresponding homopolymer is lost.

Both the monomers, $[Os(bpy)_2(mab)]^{2+}$ and $[Ru(dab)_2(mab)]^{2+}$, and homopolymers, PS−Os_{20} and PS−Ru_{20}, display nonexponential kinetics in PMMA, although the degree of nonexponential behavior is significantly less in the monomers. Nonexponential decay kinetics are a common feature for polypyridyl complexes in a variety of rigid media where it has been attributed to the heterogeneity of the solvent.[18] In short, the distribution of solvent microenvironments leads to a distribution of excited-state lifetimes. Here it appears that in the case of the polymers, solvent heterogeneity plays only part of the role in the observed nonexponential kinetics.

In PMMA, the emission spectra for the PS−Ru_{20} or PS−Os_{20} polymers change with time after photoexcitation. When monitored on the low energy side of emission band, the Os* emission from PS−Os_{20} is single exponential and similar to fluid CH_3CN. Nonexponential decay kinetics becomes prominent at the emission band maximum and to the high energy side. Reconstruction of the emission band from the single wavelength kinetic traces reveals a spectral shift as a function of time (Figure 4). The band maximum shifts ∼50 nm to the red, reaching its final form by about 10 ns. No monitoring wavelength dependence is observed for $[Os(bpy)_2(mab)]^{2+}$ in PMMA, i.e., the emission band decays uniformly with time (Figure 5).

The absence of a spectral shift for $[Os(bpy)_2(mab)]^{2+}$ in PMMA is telling. At the low concentration of monomer doping, the probability that multiple complexes occupy the same site is negligible. The polymer arrays, on the other hand, have a high *local* concentration of chromophores. One of the consequences of this high concentration is already known; close contact of adjacent sites leads to weak electronic coupling and enables Os* → Os energy transfer even in the rigid, low dielectric environment of PMMA. Another consequence is that an MLCT excited state experiences an electrostatic interaction with surrounding metal dications, counterions, in addition to the surrounding PMMA matrix. The presence of the nearby ions can significantly affect the energetics of the MLCT excited state in a way not present in monomer doped films. Because the distance between nearest neighbors and the number of metal complexes that exist in close contact varies along the chain, there is a dispersion in Os* excited-state energies.

The combination of facile energy transfer and energetic disorder leads to a situation where excited-state energy can relax from higher energy sites to lower ones as the energy migrates spatially along the polymer array (Figure 6). In the case of the PS−Os_{20}, MLCT photoexcitation of Os is followed by multiple Os* → Os energy transfer events whereby energy cascades to lower energy sites. In PS−Os_{20}, the lowest energy sites can be accessed. In the mixed polymer PS−$Ru_{17}Os_3$ the Os are deep traps, surrounded by Ru. Thus, energy transfer from Ru* → Os is irreversible and many low-energy Os sites are not reached. Correspondingly, the emission max is to higher energy.

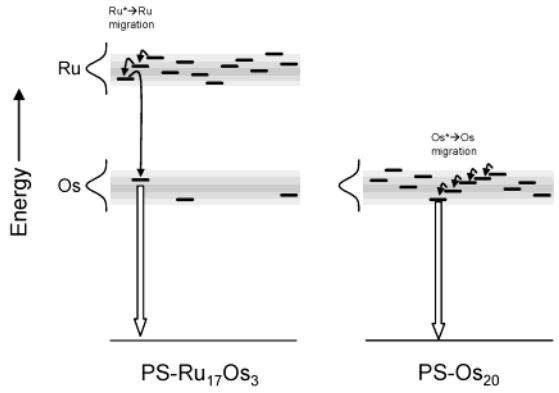

Figure 6. Schematic diagram depicting the energetic disorder contained in the PS−$Ru_{17}Os_3$ and PS−Os_{20} polymer systems. In the mixed loaded system, energy migration among the Ru sites occurs until energy transfer to an Os trap, whose excited-state energy can be anywhere within the broad Os* energy distribution. In the PS−Os_{20} system energy migration among the Os sites funnels the excited states toward lower energy sites.

Energetic disorder and excitation dependent kinetics are characteristic features of amorphous polymer media. This behavior has been observed in both singlet and triplet energy transfer in polymer films with pendant aromatic chromophores. Fayer et al.[19] studied the excitation wavelength-dependent fluorescence depolarization in the 2-vinylnaphthalene/methyl methacrylate copolymer and attributed the observed wavelength dependence to site inhomogeneity. Time-resolved phosphorescence spectra have also revealed similar information.[20]

Dynamical solvent effects involving structural reorganization of the environment in response to the excited-state charge distribution could also contribute to the spectral shift. It is possible that if the excited state were fixed (i.e., no energy migration) than a spectral shift could still be observed as a result of solvation dynamics that occur on a time scale comparable to excited-state decay. These could come in two forms, either relaxation of the surrounding PMMA shell or mobility of the polymer array. In the case of rigid, polymeric solvents such as PMMA, large amplitude motion of the polymer backbone is most likely frozen on the time scale of excited-state decay and will not participate in a solvation process involving rotation or translation. The primary glass transition temperature for the PMMA used in this study is 120 °C. However, PMMA has a very broad secondary phase transition involving motion of the ester side chain centered at room temperature. Orientational freedom of the ester group could participate in the solvation dynamics and lead to the observed time dependence. The absence of spectral shift in $[Os(bpy)_2(mab)]^{2+}$ suggests that the PMMA motion is fast (<100 ps) and not contributing to the observed dynamics which take place on a nanosecond time scale in the PS−Os_{20} system. The mobility of the polymer array is, on the other hand, still an open question. Direct excitation of the Os sites (at 700 nm) in PS−$Ru_{17}Os_3$ could provide insight into this issue.

Acknowledgment. Funding for this project was provided by The Research Corporation (RI0048), the Petroleum Research Fund (36385-G6), the United States Department of Energy, and the National Science Foundation (CHE-0301266).

References and Notes

(1) Webber, S. E. *Chem. Rev.* **1990**, *90*, 1469−1482.
(2) Holden, D. A.; Guillet, J. E. *Macromolecules* **1980**, *13*, 289.
(3) Ng, D.; Guillet, J. E. *Macromolecules* **1982**, *15*, 724.
(4) Watkins, D. M.; Fox, M. A. *J. Am. Chem. Soc.* **1996**, *118*, 4344−4353.
(5) Clements, J. H.; Webber, S. E. *J. Phys. Chem. B* **1999**, *103*, 9366.
(6) Clements, J. H.; Webber, S. E. *J. Phys. Chem. A* **1999**, *103*, 2513−2523.
(7) Jones, W. E.; Baxter, S. M.; Strouse, G. F.; Meyer, T. J. *J. Am. Chem. Soc.* **1993**, *115*, 7363−7373.
(8) Yekta, A.; Spiro, J. G.; Winnik, M. A. *J. Phys. Chem. B* **1998**, *102*, 7960−7970.
(9) Schillén, K.; Yekta, A.; Ni, S.; Winnik, M. A. *Macromolecules* **1998**, *31*, 210−212.
(10) Rharbi, Y.; Yekta, A.; Winnik, M. A.; DeVoe, R. J.; Barrera, D. *Macromolecules* **1999**, *32*, 3241−3248.
(11) Fleming, C. N.; Maxwell, K. A.; Meyer, T. J.; Papanikolas, J. M. *J. Am. Chem. Soc.* **2001**, *123*, 10336−10347.
(12) Gaines, G. L.; O'Neil, M. P.; Svec, W. A.; Niemczyk, M. P.; Wasielewski, M. R. *J. Am. Chem. Soc.* **1991**, *113*, 719−721.
(13) Chen, P.; Meyer, T. J. *Inorg. Chem.* **1996**, *35*, 5520−5524.
(14) Reisfeld, R.; Zusman, R.; Cohen, Y.; Eyal, M. *Chem. Phys. Lett.* **1988**, *147*, 142−147.
(15) Deshpande, A. V.; Namdas, E. B. *J. Lumin.* **2000**, *91*, 25−31.
(16) Chen, P.; Meyer, T. J. *Chem. Rev.* **1998**, *98*, 1439−1477.
(17) Wrighton, M. S.; Morse, D. L. *J. Am. Chem. Soc.* **1974**, *96*, 998.
(18) Maruszewski, K.; Strommen, D. P.; Kincaid, J. R. *J. Am. Chem. Soc.* **1993**, *115*, 8345.
(19) Stein, A. D.; Peterson, K. A.; Fayer, M. D. *J. Chem. Phys.* **1990**, *92*, 5622−5635.
(20) Hisada, K.; Ito, S.; Yamamoto, M. *J. Phys. Chem. B* **1997**, *101*, 6827−6833.